Universal hadronization condition in heavy ion collisions at $\sqrt{s_{\rm NN}}=62~{\rm GeV}$ and at $\sqrt{s_{\rm NN}}=2.76~{\rm TeV}$

Michal Petráň and Johann Rafelski
Department of Physics, The University of Arizona, Tucson, Arizona 85721, USA
(Dated: April 25, 2013)

We obtain a detailed description of all available hadron multiplicity yields in central Pb–Pb collisions at LHC measured in the rapidity interval |y| < 0.5. We find that the hadronization of the fireball at LHC occurs at nearly identical intensive physical bulk conditions for all centralities similar to those seen already at RHIC.

PACS numbers: 25.75.Nq, 24.10.Pa, 25.75.-q, 12.38.Mh

Introduction and motivation: We extend the successful description of central rapidity particle yields in a single freeze-out model [1, 2] to characterize the physical properties of the hadronizing fireball. We consider, as an example, a supercooled quark—gluon plasma (QGP) disintegrating into hadrons which can scatter but preserve the stable particle abundance. Therefore hadron particle multiplicities directly characterize the properties of the fireball. Final state hadrons are thus produced according to the accessible phase space with otherwise equal reaction strength. Accordingly, the particle yields are described by the chemical non-equilibrium statistical hadronization model (SHM) [3].

In this SHM implementation within the SHAREv2.2 program, the yields of particles are given the chemical freeze-out temperature T and overall normalization dV/dy (paralleling the experimental data available as dN/dy). We include phase space occupancies γ_q, γ_s for light (q = u, d) and strange s quark flavors, respectively, and we account for the small asymmetry between particles and anti-particles by fugacity factors λ_q, λ_s and the light quark asymmetry λ_{I3} . These parameters enter the distribution function as $f_i(\varepsilon, T, \gamma_i, \lambda_i) = 1/(\gamma_i^{-1}\lambda_i^{\pm 1}e^{\varepsilon/T} + S)$ for flavor i, where S = -1, 0, +1 for bosons, Boltzmann distribution and fermions respectively. We refer the reader to Section 2 of [4] for further discussion of the above parameters.

Our discussion addresses, evaluates and compares the LHC Pb–Pb experimental results available at $\sqrt{s_{NN}}=2760\,\mathrm{GeV}$ and RHIC Au–Au at $\sqrt{s_{NN}}=62.4\,\mathrm{GeV}$. We show that the chemical non-equilibrium SHM works at LHC in the 0–20% centrality. This is so, since in the chemical non-equilibrium SHM approach, we allow quark pair yield parameter $\gamma_q>1$ for light quarks; this is the key difference from the simpler equilibrium SHM. The rationale for $\gamma_q\neq 1$ originates in the high entropy density of QGP at hadronization compared to the hadron phase space in which the color degree of freedom is frozen. In case that the fireball disintegrates faster than the time necessary to equilibrate the yield of light quarks bound in hadrons, the value $\gamma_q>1$ must arise.

In case that the fireball disintegrates faster than the time necessary to equilibrate the yield of light quarks bound in hadrons, either the value $\gamma_q>1$ arises, or

one must consider a dynamical volume growth as a path for absorbing the excess entropy of QGP source. However, this second option requires a much longer lifespan of the particle source than is supported by HBT data [5, 6] and thus is experimentally excluded: the observed LHC total lifespan ($\tau_f \simeq 10\,\mathrm{fm/c}$ [6]) favors very fast, or sudden, hadronization [7, 8]. In this situation, chemical non-equilibrium approach must be applied also to the light quark abundance, introducing the light quark phase space occupancy γ_q . This proposal made for the high energy SPS data [9, 10] helped also to improve the understanding of RHIC200 hadron rapidity yield results [11] and allowed a consistent interpretation of such data across the full energy range at SPS and RHIC200 [12].

SHM fits, that arbitrarily set $\gamma_q=1$ [13, 14], (equilibrium SHM), describe hadron yields at LHC with relatively large total χ^2 . This chemical equilibrium SHM disagrees at LHC across many particle yields, but the greatest issue is the 'proton anomaly', which makes it impossible to fit the $p/\pi=0.046\pm0.003$ ratio [14] along with the multi-strange baryons Ξ and Ω .

We will show, that common intensive QGP bulk properties arise, nearly exactly equal to those found at RHIC, for all four collision centralities we analyze. We will discuss in depth the main extensive bulk property difference we find, that is the entropy dS/dy growth with energy and centrality.

Fit to most central collisions: Within the chemical non-equilibrium SHM we have, allowing for baryon-antibaryon asymmetry, seven independent statistical model parameters reduced by two constraints: a) The isospin fugacity factor λ_{I3} is constrained by imposing the charge per baryon ratio, $(\langle Q \rangle - \langle \overline{Q} \rangle)/(\langle B \rangle - \langle \overline{B} \rangle) \simeq 0.38$, present in the initial nuclear matter state at initial instant of the collision; b) For each value of λ_q , strangeness fugacity λ_s is evaluated by imposing the strangeness conservation requirement $\langle s \rangle - \langle \overline{s} \rangle \simeq 0$. Considering the particle–anti-particle symmetry at LHC, the four key parameters are the hadronization volume dV/dy, temperature T and the two phase space occupancies γ_q and γ_s . The 7th parameter is light quark fugacity λ_q .

We use as input to our fit the hadron yield data in 0–20% centrality bin as presented in Ref. [15], where a

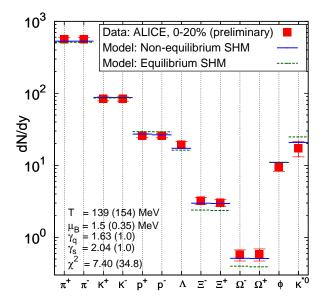


FIG. 1: (color online) The non-equilibrium SHM fit is indicated by (blue) solid horizontal lines overlaying for all the LHC-ALICE (preliminary) data available in 0-20% centrality bin (red squares). Chemical equilibrium fit is indicated by (green) dashed lines with model parameters presented in parentheses.

fit to this data set for the case of chemical equilibrium $(\gamma_s = \gamma_q = 1)$ is shown. For comparison and demonstration of method compatibility, the chemical equilibrium model fit (dashed lines in figure 1) is shown, with a large $\chi^2 = 34.8$. In both approaches, we fit the same data, the decrease in χ^2 by factor nearly 5 is due to chemical non-equilibrium i.e., $\gamma_q \neq 1$, $\gamma_s \neq 1$. We determine the best light quark fugacity factor $\lambda_q = 1.00359$, which corresponds to baryo-chemical potential $\mu_B \simeq 1.5 \, \text{MeV}$, and we apply strangeness and charge per baryon conservation by fitting them as two additional data points. The result of our 0-20% centrality bin fit is shown in figure 1 and in top section of the third column of table I. We compare our present results to our recent analysis [16] of Au–Au collisions at $\sqrt{s_{NN}} = 62.4 \, \text{GeV}$ at RHIC62, shown in the 2nd column in table I.

More peripheral centralities: We extend our study to more peripheral collisions at LHC using much smaller data set, complemented by two assumptions as follows: a) We consider the three ratios K^{*0}/K^- , $\Lambda/\pi \equiv 2\Lambda/(\pi^- + \pi^+)$ and ϕ/K^- , as presented in [17] and which we show in figure 2 with full symbols. We fit these ratios in three centrality bins, 20–40%, 40-60% and 60-80%, in which K^*/K and Λ/π have experimental data point. We take average of two neighboring ϕ/K data points in order to use this ratio as input to our fit in the intermediate centrality. This is consistent with the claim that ϕ/K is constant over all centralities and has been claimed independent of centrality in [17].

b) To obtain overall normalization, we complement the ratios with charged particle rapidity density $dN_{\rm ch}/dy$.

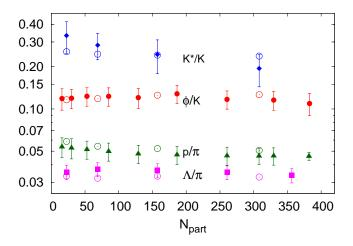


FIG. 2: (color online) Experimental data (full symbols) and model predicted (open circles) for particle ratios as a function of centrality. See text for discussion of data and results.

Based on our fit of 0–20% centrality data, we see that the ratio of charged particle rapidity to pseudo-rapidity density is $(dN_{\rm ch}/dy)/(dN_{\rm ch}/d\eta)=1.115$. We multiply data from [18] by this factor, and use the resulting $dN_{\rm ch}/dy$ as an additional data point, that determines the value of fireball volume dV/dy. The input multiplicity data is presented in the figure 3.

c) We include the yields of π^{\pm} , K^{\pm} and p^{\pm} , as presented in [19] and shown in figure 3. Similarly to ϕ/K ratio, we use as input averages of yields in two neighboring centrality bins.

We fit the three centrality bins of LHC2760 data using the eight data points and the two conservation laws, which fix λ_s and λ_{I3} . We thus have five degrees of freedom as is seen in table I in 4th, 5th and 6th column. All studied centralities show reasonable $\chi^2/\text{ndf} \leq 1.1$. We find for all four LHC centrality bins remarkably similar statistical parameters.

We compare the outcome of the fit showing the three input ratios K^{*0}/K^- , Λ/π and ϕ/K^- , and p/π in figure 2. All data are well fitted including p/π , which we evaluate from the individual fitted yields of p and π from [19].

The predicted particle yields normalized by $N_{\rm part}/2$ are shown in figure 3, where considering particle—antiparticle symmetry only one of the isospin multiplets is shown. The π ,K and p yields are fitted values, whereas the other particle yields are predictions. We indicate in figure 3 on the right edge the experimental input for the 0–20% bin with an offset to assure visibility of the small differences between fit and experimental data. We show the input multiplicity $(dN_{\rm ch}/dy)/(N_{\rm part}/2)$ and fit result in figure 3. Both are overlapping exactly for the three peripheral bins since this is the most precise input data.

Hadronization conditions: Despite a change by a factor of 45 in reaction energy comparing RHIC and LHC, and the wide range of centrality, the only quantity among statistical parameters shown in table I that significantly

TABLE I: Top section shows chemical non-equilibrium SHM fit parameters dV/dy, T, γ_q , γ_s and $\chi^2_{\rm total}$ with ndf (number data less number of parameters) obtained in each centrality bin. Errors are a fit-stability estimate obtained with K[±] yield shifted within experimental error, the underlying statistical fit error is negligible. Bottom section presents fireball bulk properties in each bin: energy density ε , pressure P, entropy density σ , strangeness per entropy content s/S, and entropy at LHC2760 compared to RHIC62, $S_{\rm LHC}/S_{\rm RHIC}$. The centrality defining number of participants N_{part} values are adopted from [20].

| | RHIC62 | LHC2760 | | | |
|--------------------------------------|--------|---------------------|---------------------|---------------------|---------------------|
| Centrality | 0-5% | 0-20% | 20-40% | 40-60% | 60-80% |
| $\langle N_{ m part} \rangle$ | 346 | 308 | 157 | 68.8 | 22.6 |
| dV/dy [fm ³] | 853 | 2455 ± 146 | 1169 ± 9 | 406 ± 3 | 102 ± 7 |
| $T [\mathrm{MeV}]$ | 139.5 | 138.6 ± 1.1 | 137.6 ± 0.03 | 140.5 ± 0.04 | 143.2 ± 0.08 |
| γ_q | 1.58 | 1.627 ± 0.007 | 1.633 ± 0.0002 | 1.616 ± 0.003 | 1.60 ± 0.02 |
| γ_s | 2.24 | 2.04 ± 0.04 | 2.01 ± 0.12 | 1.83 ± 0.08 | 1.70 ± 0.09 |
| $\chi^2_{\rm total}/{\rm ndf}$ | 0.38/5 | 7.40/8 | 2.93/5 | 3.58/5 | 5.43/5 |
| $\varepsilon [{\rm GeV/fm^3}]$ | 0.493 | 0.466 ± 0.018 | 0.441 ± 0.012 | 0.488 ± 0.010 | 0.536 ± 0.025 |
| $P \left[\mathrm{MeV/fm}^3 \right]$ | 82.0 | 79.1 ± 2.8 | 75.5 ± 1.5 | 82.2 ± 1.3 | 90.2 ± 4.0 |
| $\sigma [\mathrm{fm}^{-3}]$ | 3.40 | 3.23 ± 0.11 | 3.07 ± 0.07 | 3.36 ± 0.06 | 3.65 ± 0.13 |
| s/S | 0.0322 | 0.0296 ± 0.0002 | 0.0289 ± 0.0014 | 0.0277 ± 0.0009 | 0.0267 ± 0.0011 |
| $S_{\rm LHC}/S_{ m RHIC}$ | | 3.05 | 2.66 | 2.18 | 1.52 |

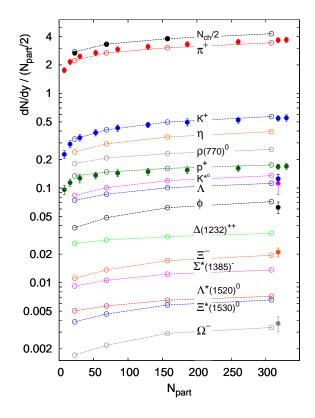


FIG. 3: (color online) Predicted particle yields per participant pair as a function of centrality. Open symbols represent our model predictions; lines guide the eye. We show experimental data for the 0–20% bin as full symbols, with an offset.

changes is dV/dy. This suggests, that we should look closer at the intensive bulk physical properties of the fireball: The emitted hadrons not only carry away from the

fireball the above discussed charge, baryon number or strangeness, but also e.g. the thermal energy, dE/dy obtained by summing the energy content of all produced particles, observed and predicted.

The bulk thermal energy density at hadronization ε defined by $\varepsilon \equiv (dE/dy)/(dV/dy)$ is of direct interest. Similarly, we evaluate the entropy dS/dy, pressure P and total yield of strangeness $ds/dy \equiv d(q_s + \bar{q}_s)/2dy$. These properties of the fireball at hadronization are shown in the bottom section of the table I, where for simplicity we omit in the first column the symbol d/dy.

As one can see by comparing the second and third columns of table I, the intensive properties of the RHIC62 fireball at hadronization i.e. ε , P, σ and s/S, are practically identical to the here evaluated case LHC2760, and this continues across all considered centralities as is seen in the 4th, 5th and 6th column of table I. We show a comparison of ε , P as a function of centrality between LHC (solid symbols) and RHIC (open symbols) in the bottom part of figure 4. The difference between LHC and RHIC can be easily attributed to the fit uncertainties, since the intensive quantities are proportional to a high power of statistical parameters.

Hadronization volume dV/dy does not characterize the early stage of a collision, this information is available in the entropy content at hadronization $dS/dy \propto dV/dy$ which presents a more accurate view of the prehadronization processes that created the fireball. For an ideally flowing and expanding QGP, most of the observed entropy yield dS/dy of a fireball is created early in the collision. In the top panel of figure 4 we see that at LHC, $dS/dy \propto N_{part}^{\sim 1.173}$, the rise is faster than linear. For comparison note that at RHIC, the entropy yield rises almost linearly with N_{part} . Last row of table I shows the enhancement of entropy at LHC compared to RHIC, $S_{\text{LHC}}/S_{\text{RHIC}}$. The enhancement decreases as a function

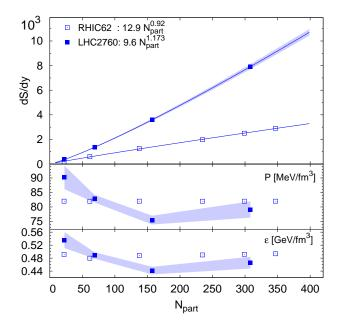


FIG. 4: (color online) Top panel shows entropy content of the fireball at LHC (full symbols) and RHIC (open symbols) as a function of centrality. Bottom part shows pressure P and energy density ε at hadronization with the same symbols for LHC and RHIC as in the top panel, for values see table I.

of centrality from ~ 3 to $\sim 1.5,$ which implies additional entropy production mechanism proportional to centrality at LHC.

Strangeness per entropy $s/S \equiv (ds/dy)/(dS/dy)$ is of particular interest in the source fireball since both entropy and strangeness yields are nearly preserved in the hadronization process, but the production of strangeness occurs after most of the entropy is created. Up to a well studied proportionality factor, s/S is the ratio of strange quark abundance to total quark and gluon abundance which is making up the entropy in the bulk. Therefore, s/S measures the degree of chemical equilibration attained in the QGP We observe a constant value of $s/S \simeq 0.03$ (see table I), which is in agreement with theoretical expectations for the strange quark mass $m_s \simeq 100\,\mathrm{MeV}$ [21].

Comments and Conclusions: The LHC2760 experimental environment has opened a new opportunity to investigate in detail the hadron production mechanisms. Precise particle tracking near to interaction vertex in the ALICE removes the need for off-line corrections of weak interaction decays, and at the same time, vertex tracking enhances the efficiency of track identification, increasing considerably the precision of particle yield measurement [13, 15]. All LHC experimental results used in the present work were obtained in this way by the ALICE experiment for Pb–Pb collisions at $\sqrt{s_{NN}} = 2.76$ TeV, limited to the central unit of rapidity interval -0.5 < y < 0.5.

In this new experimental environment we show the

necessity to introduce the final state hadron chemical non-equilibrium, which describes well all experimental results obtained in the Pb–Pb collisions at $\sqrt{s_{NN}}=2.76\,\mathrm{TeV}$ from LHC. As figure 1 shows, $\gamma_q\simeq 1.6$ (non-equilibrium of light quarks) allows to describe the ratio p/ $\pi=0.046\pm0.003\,[13,14]$ together with yields of multistrange baryons Ξ and Ω .

Another approach to describe the data including the 'anomalous' proton yield at LHC involves chemical equilibrium hadronization at relatively high T followed by hadron interactions [22, 23]. We note the chemical equilibrium SHM yields at hadronization in figure 1, which overpredict proton yield, and at the same time underpredict both Ξ and Ω . Any alternate data explanation must come to terms with this situation, thus it must deplete protons and enhance both Ξ and Ω , and at the same time the ratio p/ π must remain practically constant . This is difficult, as we now discuss, looking closer at the results of Ref. [22, 23]:

- we see in figure 1 of [22] that if and when equilibrium style hadronization occurs and leads to high T the necessary post-hadronization reactions deplete protons and Ξ and enhance of Ω . This means that the already too small a yield of Ξ is further depleted and disagrees gravely with experiment.
- the measured p/ π ratio in the 0–5% centrality bin can be made consistent with post-hadronization proton–antiproton annihilation [23]. This fine tunes model parameters and as a result for the 20–30% centrality bin Ref. [23] reports increased p/ $\pi=0.058$.
- the model predicts for peripheral collisions yet less annihilation and thus a p/π ratio approaching equilibrium SHM value, which is twice as large as experiment. While experiment for p/π seen in figure 2 is a constant for all centralities, Ref. [23] thus predicts a rapid variation by about factor of two.

These arguments lead to the conclusion that post-hadronization interactions are inconsistent with the experimental data of baryon yields at LHC. On the other hand, our chemical non-equilibrium SHM at LHC produces a high confidence level fit $\chi^2/\text{ndf} = 7.4/8 < 1$. Prior SPS and RHIC data analysis [11, 12, 16] has already strongly favored chemical non-equilibrium variant of SHM. The implied sudden hadronization picture is perfectly consistent with the anisotropic flow of quarks leading to the final hadron momentum distribution azimuthal asymmetry (see e.g. [25]).

Moreover, we find that LHC and RHIC results are quite consistent in our approach, we obtain the same hadronization condition (ε, P, σ) at LHC as previously reported at RHIC, which in turn agrees with high energy SPS [12]. The energy density of hadronizing matter is 0.50 ± 0.05 GeV/fm³, which is about 3.3 times the energy density of nuclear matter, the pressure is $P = 82 \pm 8 \,\mathrm{MeV/fm^3} = (158 \pm 4 \,\mathrm{MeV})^4$, as is seen in the bottom part of figure 4, and which has been proposed in [26]. The bottom part of table I also shows that the entropy density is constant: $\sigma = 3.35 \pm 0.30 \,\mathrm{fm^{-3}}$ for

both experiments and all centralities.

These typical QGP properties, including $s/S \rightarrow 0.03$, mean that at LHC, the source of hadrons is a chemically equilibrated strangeness saturated QGP fireball. Furthermore, the universal hadronization condition cannot be

viewed anymore as being due to successive particle emission, or to proceed via equilibrated hadron gas phase.

Acknowledgments: Work supported by a grant from the U.S. Department of Energy, DE-FG02-04ER41318.

- M. Rybczynski, W. Florkowski and W. Broniowski, Phys. Rev. C 85, 054907 (2012) [arXiv:1202.5639 [nucl-th]].
- [2] W. Broniowski and W. Florkowski, Phys. Rev. Lett. 87, 272302 (2001) [nucl-th/0106050].
- [3] G. Torrieri, S. Steinke, W. Broniowski, W. Florkowski, J. Letessier, J. Rafelski, Comput. Phys. Commun. 167, 229-251 (2005). [nucl-th/0404083]; and G. Torrieri, S. Jeon, J. Letessier, J. Rafelski, Comput. Phys. Commun. 175, 635-649 (2006). [nucl-th/0603026].
- [4] J. Rafelski, Eur. Phys. J. ST 155 (2008) 139 [arXiv:0710.1931 [nucl-th]].
- [5] L. P. Csernai, M. I. Gorenstein, L. L. Jenkovszky, I. Lovas and V. K. Magas, Phys. Lett. B 551, 121 (2003) [hep-ph/0210297].
- [6] K. Aamodt et al. [ALICE Collaboration], Phys. Lett. B 696, 328 (2011) [arXiv:1012.4035 [nucl-ex]].
- [7] L. P. Csernai and I. N. Mishustin, Phys. Rev. Lett. 74, 5005 (1995).
- [8] J. Rafelski and J. Letessier, Phys. Rev. Lett. 85, 4695 (2000) [hep-ph/0006200].
- [9] J. Letessier and J. Rafelski, Phys. Rev. C 59, 947 (1999) [hep-ph/9806386].
- [10] J. Letessier and J. Rafelski, Int. J. Mod. Phys. E 9, 107 (2000) [nucl-th/0003014].
- [11] J. Rafelski, J. Letessier and G. Torrieri, Phys. Rev. C 72, 024905 (2005) [nucl-th/0412072].
- [12] J. Letessier and J. Rafelski, Eur. Phys. J. A 35, 221 (2008) [nucl-th/0504028].
- [13] B. Abelev [ALICE Collaboration], arXiv:1209.3285 [nuclex]. Proceedings from Physics of the LHC 2012 Confer-

- ence, Vancouver, BC
- [14] B. Abelev et al. [ALICE Collaboration], Phys. Rev. Lett. 109 (2012) 252301 [arXiv:1208.1974 [hep-ex]].
- [15] Quark Matter 2012 International Conference (QM 2012), August 13-18, 2012, Washington, DC, USA, M. Ivanov: Results on identified particle spectra from ALICE
- [16] M. Petran, J. Letessier, V. Petracek and J. Rafelski, Acta Phys. Polon. Supp. 5, 255 (2012) [arXiv:1112.3189 [hepph]].
- [17] S. Singha [ALICE Collaboration], arXiv:1211.0187 [hep-ex].
- [18] K. Aamodt et al. [ALICE Collaboration], Phys. Rev. Lett. 106, 032301 (2011) [arXiv:1012.1657 [nucl-ex]].
- [19] B. Abelev et al. [ALICE Collaboration], arXiv:1303.0737 [hep-ex].
- [20] B. Abelev *et al.* [ALICE Collaboration], arXiv:1301.4361 [nucl-ex].
- [21] I. Kuznetsova and J. Rafelski, Eur. Phys. J. C 51, 113 (2007) [hep-ph/0607203].
- [22] J. Steinheimer, J. Aichelin, M. Bleicher and Phys. Rev. Lett. 110, 042501 (2013) [arXiv:1203.5302 [nucl-th]].
- [23] I. A. Karpenko, Y. M. Sinyukov and K. Werner, Phys. Rev. C 87, 024914 (2013) [arXiv:1204.5351 [nucl-th]].
- [24] W. Brueckner, et al., Zeitschrift für Physik A Atomic Nuclei, 335, 2 (1990), 217-229
- [25] U. WHeinz and R. Snellings, arXiv:1301.2826 [nucl-th].
- [26] J. Rafelski and J. Letessier, J. Phys. G G **36**, 064017 (2009) [arXiv:0902.0063 [hep-ph]].